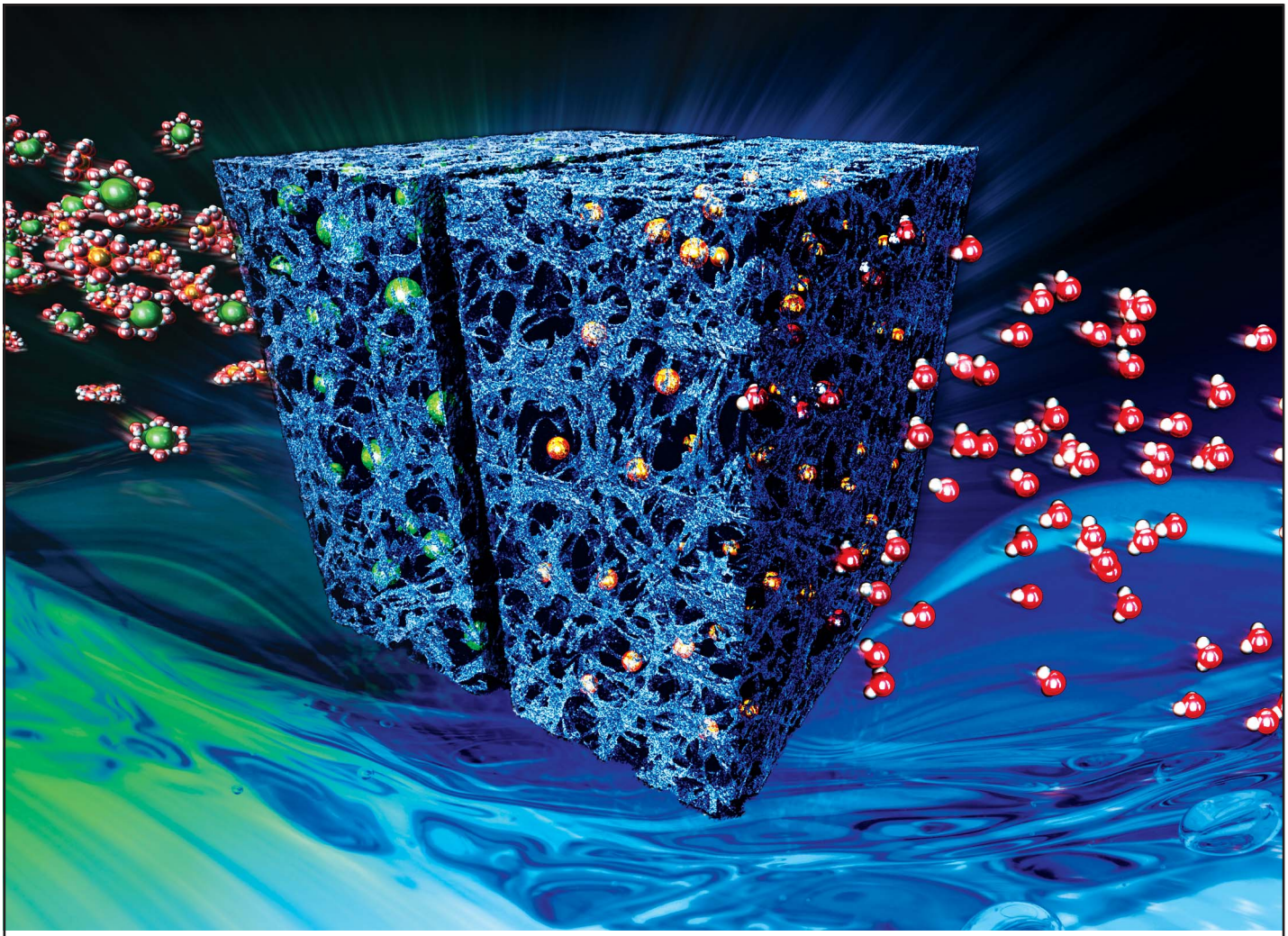

Showcasing research from the Lawrence Livermore National Laboratory and Stanford University.

Title: Capacitive desalination with flow-through electrodes

Capacitive desalination is a promising desalination technique. A novel flow-through electrode architecture utilizes a newly developed porous carbon material to achieve dramatic improvements in desalination rate and salt concentration reduction. Image depicts a capacitive desalination cell with a flow-through architecture.

As featured in:

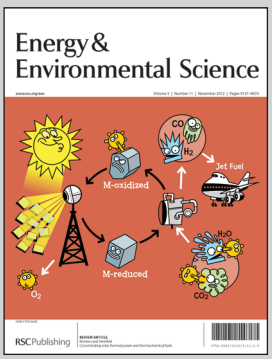

See Santiago, Stadermann *et al.*, *Energy Environ. Sci.*, 2012, **5**, 9511.

RSC Publishing

www.rsc.org/ees

Registered Charity Number 207890

Energy & Environmental Science

Dynamic Article Links

Cite this: *Energy Environ. Sci.*, 2012, **5**, 9511

www.rsc.org/ees

PAPER

Capacitive desalination with flow-through electrodes†

Matthew E. Suss,[ab] Theodore F. Baumann,[b] William L. Bourcier,[b] Christopher M. Spadaccini,[b] Klint A. Rose,[b] Juan G. Santiago*[a] and Michael Stadermann*[b]

Received 27th February 2012, Accepted 26th June 2012
DOI: 10.1039/c2ee21498a

Capacitive desalination (CD) is a promising desalination technique as, relative to reverse osmosis (RO), it requires no membrane components, can operate at low (sub-osmotic) pressures, and can potentially utilize less energy for brackish water desalination. In a typical CD cell, the feed water flows through the separator layer between two electrically charged, nanoporous carbon electrodes. This architecture results in significant performance limitations, including an inability to easily (in a single charge) desalinate moderate brackish water feeds and slow, diffusion-limited desalination. We here describe an alternative architecture, where the feed flows directly through electrodes along the primary electric field direction, which we term flow-through electrode (FTE) capacitive desalination. Using macroscopic porous electrode theory, we show that FTE CD enables significant reductions in desalination time and can desalinate higher salinity feeds per charge. We then demonstrate these benefits using a custom-built FTE CD cell containing novel hierarchical carbon aerogel monoliths as an electrode material. The pore structure of our electrodes includes both micron-scale and sub-10 nm pores, allowing our electrodes to exhibit both low flow resistance and very high specific capacitance (>100 F g^{-1}). Our cell demonstrates feed concentration reductions of up to 70 mM NaCl per charge and a mean sorption rate of nearly 1 mg NaCl per g aerogel per min, 4 to 10 times higher than that demonstrated by the typical CD cell architecture. We also show that, as predicted by our model, our cell desalinates the feed at the cell's RC timescale rather than the significantly longer diffusive timescale characteristic of typical CD cells.

Introduction

Desalination of seawater and saline aquifers is among the processes critical to ensuring a safe and adequate freshwater supply.[1] Currently, the majority of worldwide desalination capacity is contributed by reverse osmosis (RO) desalination plants.[1] Capacitive desalination (CD), also known as capacitive deionization (CDI), is a promising water desalination technique relative to reverse osmosis (RO) because it can operate with low (sub-osmotic) feed pressures, requires no membrane components, and is potentially more energy efficient for desalination of brackish waters.[2–5] In a CD cell, a pair of porous electrodes are electrically charged to drive the uptake of salt ions by pore surface electric double layers (EDLs).[6] The electrodes are typically carbon based, and one of the most widely used electrode

[a]*Stanford University, Department of Mechanical Engineering, 440 Escondido Mall, Stanford, CA, USA. E-mail: juan.santiago@stanford.edu; Fax: +1 650 723 7657; Tel: +1 650 723 5689*
[b]*Lawrence Livermore National Laboratory, 7000 East Avenue, Livermore, CA, USA. E-mail: stadermann2@llnl.gov; Tel: +1 925 423 9128*
† Electronic supplementary information (ESI) available. See DOI: 10.1039/c2ee21498a

Broader context

Capacitive desalination (CD) is an attractive alternative to typical desalination techniques, such as reverse osmosis, as it requires no membrane components, can operate at low (sub-osmotic) pressures, and is potentially more energy efficient at brackish water salinities. Traditional capacitive desalination systems suffer from slow, diffusion-limited desalination and low concentration reductions per charge, limiting their applicability. The novel flow-through electrode (FTE) cell developed and characterized in this study allows for vast improvements in capacitive desalination performance. We demonstrate a 4–10 times faster salt removal rate relative to traditional capacitive desalination systems while achieving higher feed concentration reductions of up to 70 mM per charge. We also use model and experimental results to show that desalination in our FTE cell is not diffusion-limited. The physical insights and cell architecture presented here will allow for future CD devices to better leverage the performance benefits inherent in desalination with a capacitor.

materials is carbon aerogel due to its high specific surface area and monolithic structure.[3,5]

CD systems are most often designed such that the feed stream to be desalinated flows primarily between the two porous charging electrodes.[2,3,36] We term this typical architecture a "flow between" (FB) CD system and depict this schematically in Fig. 1a. Current FB systems have significant limitations, including an inability to easily (in a single charging step) desalinate moderate brackish water feeds and long times required for desalination.[2] For example, FB CD systems typically reduce the concentration of a sodium chloride feed solution by less than 20 mM per charge,[2,5,7,8] whereas seawater has an ionic strength of about 700 mM.[9] Also, desalination of the feed in a FB CD system can require over an order of magnitude longer than the charging time of the cell.[2] Further, in FB cells, the separator layer between electrodes must serve as both a flow channel and a structure to prevent electrical shorts between the two porous electrodes.[2] This complicates cell design, as the thickness (along the electric field direction) of the separator must be carefully optimized to minimize the cell electrical resistance and volume while allowing a sufficiently large area for efficient fluid flow.

An alternative cell architecture which can address these limitations is to flow the feed stream directly through electrode pores, which we term "flow-through electrode" (FTE) CD and have shown this schematically in Fig. 1b. There is a dearth of work with CD systems employing FTEs. Early work on CD by Johnson *et al.* utilized FTEs of unconsolidated charcoal.[10,11] However, they observed significant electrode degradation after repeated desalination cycles.[10] Also, their electrodes were composed of carbon particles of diameters of the order of a hundred microns, and the particles themselves contained micropores.[11] This morphology hindered cell regeneration times. For example, they estimated that >3 min were required to allow salt concentration within particle micropores to reach

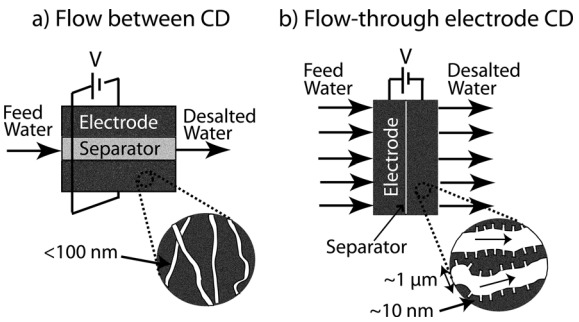

Fig. 1 (a) Schematic representation of a typical flow between (FB) capacitive desalination cell, where the feed water flows between electrodes through a porous separator element. The electrodes in FB cells often consist of nanoscale pores which maximize the surface area but prevent flow through the electrodes. Desalination thus involves transport of salt from the separator space into electrode pores (a distance of typically order 100 μm). (b) Schematic representation of a flow-through electrode (FTE) capacitive desalination cell, where the feed water flows directly through electrode pores. The FTE cell uses low hydraulic resistance, high surface area porous electrodes with hierarchical porosity, consisting of micron-scale pores and nano-scale pores. Thus, desalination requires the transport of salt from the micron-scale pore bulk to the nanoscale pore (a distance on the order of 1 μm).

equilibrium with the solution flowing in the local particle interstitial space.[11] To our knowledge, the next study utilizing an FTE type architecture, nearly 4 decades later, was the recent series of works by Avraham *et al.* and Cohen *et al.*, using activated carbon cloth electrodes.[12–15] Avraham *et al.* attributed choice of the FTE type architecture to compatibility and convenience associated with small-scale fundamental experiments to quantify electrode charge efficiency. Thus, previous CD systems employing FTEs utilized either non-monolithic electrode materials which were unstable[10,11] or materials typically associated with FB systems.[12–15] There has been little work on developing and optimizing electrode materials specifically for the unique set of requirements or opportunities presented by FTE systems. Additionally, the potential benefits of FTE systems *vs.* common FB systems have not been clearly elucidated, modelled, or demonstrated.

While traditional carbon aerogels are among the most commonly used electrode materials in FB CD systems, they are not appropriate as FTEs as their pore diameters are typically sub-50 nm, and thus the electrodes exhibit a prohibitively high hydraulic resistance to flow.[3,5,16] Recently developed hierarchical carbon aerogel monoliths (HCAMs),[17] by contrast, represent a more attractive choice for FTE CD electrodes due to their unique bimodal pore structure. These materials possess a continuous micron-scale pore network, into which size-tuneable nanopores are etched by thermal activation.[17] As a result, HCAMs simultaneously provide high specific capacitance (>100 F g^{-1}) and low hydraulic resistance.[18] To our knowledge, HCAM materials have not been investigated as CD electrodes prior to the current work.

In this work, we use macroscopic porous electrode theory to investigate and quantify the benefits of FTE *vs.* the commonly used FB architecture. As we shall discuss, the basic architecture of FTE cells allows for fast desalination at resistive–capacitive (RC) timescales, rather than longer diffusive timescales required for FB CD cells, as well as stronger reductions in feed salt concentration per charge. Further, to demonstrate the potential benefits of FTE CD, we built and characterized the performance of a FTE CD cell utilizing HCAM electrodes, and to our knowledge this is the first time this newly developed material has been used in a CD cell. Also, the separator of our FTE cell is not the primary flow channel (as in FB CD); thus we were able to minimize the separator thickness (in the electric field direction) to 1% of that of the electrode–separator assembly. This relative thickness is much smaller than the 100% or higher relative thicknesses of typical FB systems.[2,5,7,19] A relatively thin separator is a key characteristic which allows FTE CD cells to achieve optimized desalination performance and improved reductions in salt concentration per charge.

Theory

We here leverage macroscopic porous electrode (MPE) theory to elucidate and contrast desalination performance in FB and FTE CD systems. MPE theory allows for a formulation of transport equations based on volume averaged variables, where averaging occurs over dimensions significantly larger than pore diameters yet small compared to the electrode dimensions.[20] Thus, MPE models can be used to predict the spatiotemporal concentration and potential in a CD cell, while neglecting the often complex

geometrical details of the pore structure.[6,11] MPE theory was first applied to CD electrodes by Johnson and Newman,[11] and was recently extended to include the effects of transient Gouy–Chapman–Stern EDL charging by Biesheuvel and Bazant.[6]

We here consider a one-dimensional model of a charging, stopped-flow CD cell, where the salt solution in the CD cell is quiescent. Further, we model the effects of transient EDL charging using a simple Helmholtz model for the EDL structure.[11,21] See Appendix A in the ESI† for details of the model derivation. We later demonstrate that the desalination timescale trends predicted by our simple model match those observed in our data (see Results and discussion section), and help explain observations reported by others. However, we emphasize that our model is not appropriate to predict exact cell performance. For example, using the Helmholtz model implies a linear EDL capacitance and unity charge efficiency, which is typically not the case for CD electrodes.[6,22] The true EDL structure at the high voltages used in CD cells (typically up to 500–750 mV across the EDL) is a topic of active research, and there has been significant theoretical work in this area.[23–26] In our model, we further assume a dilute binary and symmetric salt with equal anion and cation mobilities. We furthermore neglect the effects of surface (tangential) conduction or electroosmotic flow. For these conditions, the equations governing the evolution of pore bulk (outside the EDL) liquid concentration, c, and pore bulk electric potential, ϕ, in a system with two electrodes and a separator are:

$$\frac{\partial c}{\partial t} = D\frac{\partial^2 c}{\partial x^2} - f(x)\frac{C}{2\psi F z_{\text{count}}}\frac{\partial \phi}{\partial t}, \tag{1}$$

$$f(x)\frac{\partial \phi}{\partial t} = \frac{\psi}{C}\frac{\partial}{\partial x}\left(\sigma\frac{\partial \phi}{\partial x}\right), \tag{2}$$

$$f(x) = H(x) - H(x - l_e) + H(x - l_e - l_s). \tag{3}$$

Here l_e is the thickness of the positive and negative electrode, and l_s is the thickness of the separator between electrodes. The function $f(x)$ is defined as zero in the separator, and unity inside the electrodes, where $H(x)$ is a Heaviside step function.‡ Also, D is the anion and cation diffusivity, which is typically lower in the electrode pore space than in free solution,[6] C is the electrode capacitance per electrode volume (*e.g.*, in units F cm^{-3}), σ is the pore bulk electrolyte conductivity, z_{count} is the valence of the counterion (to the local wall charge), and ψ is the porosity of both the separator and the electrodes (assumed to be equal).

The equations governing pore bulk concentration and potential (eqn (1) and (2)) are similar to the simple 1D heat equation, except that eqn (1) contains a sink term (last term on the right) which couples the two equations, and eqn (2) has a non-uniform, non-constant diffusivity-like parameter (ion conductivity, σ). Eqn (2) shows that potential evolves from its initial distribution in a diffusion-like manner with a diffusivity of $\psi\sigma/C$ (termed an "electrical diffusivity"[11]), until the initial electric field is fully screened by EDL ions. Further, σ can be reduced locally by cell charging *via* desalination, and this acts to slow down the screening process. In the absence of any significant desalination, eqn (2) is decoupled from eqn (1), and porous electrode charging proceeds according to an RC timescale.[6,27] By accounting for the ionic resistance of both the electrodes and separator, we can formulate the following RC timescale for our CD cell (see Appendix A in the ESI† for derivation):

$$\tau_{RC} = \frac{Cl_e^2 T}{\psi\sigma_o}\left(1 + \frac{l_s}{2l_e}\right), \tag{4}$$

where σ_o is the initial pore bulk conductivity (prior to desalination) in the cell and T is the tortuosity (assumed to be equal for the separator and electrode). The boundary conditions used in solving this model are the following:

$$\left.\frac{\partial c}{\partial x}\right|_{x=0} = \left.\frac{\partial \phi}{\partial x}\right|_{x=0} = 0, \tag{5}$$

$$\left.\frac{\partial c}{\partial x}\right|_{x=2l_e+l_s} = \left.\frac{\partial \phi}{\partial x}\right|_{x=2l_e+l_s} = 0, \tag{6}$$

$$c(x, t=0) = c_o, \tag{7}$$

$$\begin{aligned}\phi(x, t=0) &= -\frac{V}{2} \quad 0 \le x \le l_e \\ &= \frac{V}{l_s}x - \frac{V}{2}\left(1 + \frac{2l_e}{l_s}\right) \quad l_e \le x \le l_e + l_s \\ &= \frac{V}{2} \quad l_e + l_s \le x \le 2l_e + l_s,\end{aligned} \tag{8}$$

where V is the voltage applied to the cell (which is evenly distributed between the symmetric electrodes). The boundary conditions given by eqn (5) and (6) are due to zero salt flux and zero ionic current between the current collector and the adjacent bulk liquid in the electrode's pores. That is, we assume the current collector has zero capacitance (no charging current to the current collector), and assume no faradaic reactions at the current collector. Notably, our boundary conditions do not assume fixed salt concentration far from the electrode,[6] but allow the salt concentration in our finite separator to evolve freely in response to depletions within the electrodes. The initial conditions are uniform concentration, c_o, throughout the cell (eqn (7)) and the suddenly applied step voltage dropped entirely across the separator layer (eqn (8)).[6]

We solved the model at conditions typical of FB CD cells to gain insight into the timescales involved in desalination. The geometry we used is representative of typical FB CD systems: 0.5 mm thick electrodes and a 0.5 mm thick separator. We depict the relative layer thicknesses and positions as grey blocks just above Fig. 2a. We used a typical electrode capacitance of 25 F cm^{-3} (see Appendix B in the ESI†), applied voltage of 1 V, porosity of 0.75, valence of 1, ion diffusivity of 2×10^{-9} m^2 s^{-1} (the approximate value for chloride ions in free solution), and a tortuosity of 1. The coupled equations for concentration and potential were solved with commercially available finite element simulation software (Comsol Multiphysics 3.5, Burlington, USA).

In Fig. 2, we plot example model results of the evolution of concentration and potential for $c_o = 100$ mM. We plot solutions at $t = 0$, $0.25\tau_{RC}$, τ_{RC}, τ_D, and at the steady state, t_{ss}. τ_{RC} was calculated from eqn (5) above, and $\tau_D = l_s^2/4D$ represents the diffusion time across the separator half-thickness (where

‡ Interestingly, Heaviside innovated the transmission line circuit model, which is commonly applied to charging porous electrodes.[27,35]

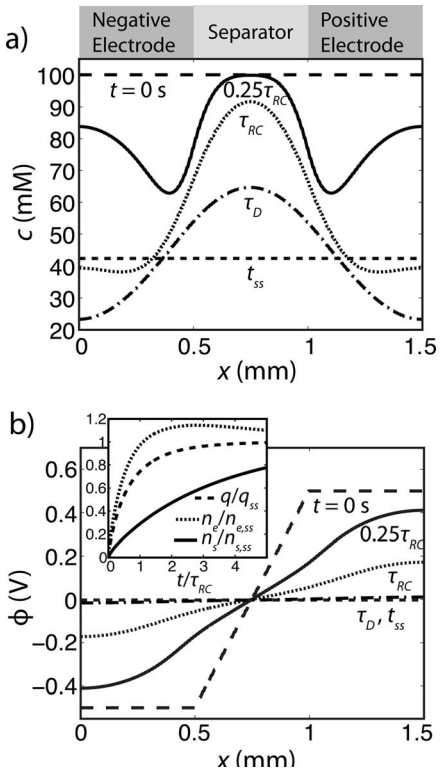

Fig. 2 Model predictions for the evolution of (a) salt concentration and (b) electric potential in a stopped-flow CD cell. The cell consists of two 0.5 mm thick electrodes and a 0.5 mm thick separator, as shown schematically above (a), and is initially filled with a 100 mM salt solution. We apply 1 V to the electrodes at $t = 0$, and plot the predictions at $t = 0.25\tau_{RC}$ (solid line), τ_{RC} (dotted line), τ_D ($\sim 4\tau_{RC}$) (dashed dotted line), and at the steady state (short dashed line). The initial condition (long dashed line) is also shown. At times on the order of τ_{RC}, the electrodes' pore bulk is desalinated and potential gradients are strongly suppressed throughout the cell. However, at this time the separator region shows only slight desalination. At later times, on the order of τ_D, desalination of the separator continues *via* molecular diffusion of the salt into the depleted electrode pores. The inset plot of (b) summarizes the dynamics of the charging process, showing that EDL charging and electrode pore desalination (q/q_{ss} and $n_e/n_{e,ss}$) occur at RC timescales, while separator pore desalination ($n_s/n_{s,ss}$) requires a significantly longer time.

$\tau_D \sim 4\tau_{RC}$). At $t = 0.25\tau_{RC}$ (solid line) and τ_{RC} (dotted line), the salt concentration in the electrode pore space (Fig. 2a) and electric potential gradients in the separator pore space (Fig. 2b) have each decreased significantly relative to their initial values (dashed line). For example, at τ_{RC}, the concentration in the electrode pore space has been reduced to about 40 mM, and the electric field is roughly 0.25 V mm^{-1} in the separator, reduced from 2 V mm^{-1}. In contrast, at τ_{RC}, the salt concentration in the separator pore space has only been reduced slightly to between 80 and 90 mM. The charging of the electrodes within about the τ_{RC} timescale strongly suppresses the electric field in the system. Thereafter, the transport of salt ions is largely governed by molecular diffusion. At $t = \tau_D \sim 4\tau_{RC}$ (dashed-dotted lines), the salt concentration in the (now near zero field) separator region is reduced to values between about 50 and 65 mM, consistent with salt slowly diffusing from the separator into the depleted electrode pores. At the steady state (short-dashed line), diffusion has a homogenized salt concentration of about 40 mM throughout. The inset in Fig. 2b summarizes the dynamics of the charging process. Here, we plot the normalized charge stored in the EDL, q/q_{ss}, the normalized moles of salt removed from the electrodes' pore bulk, $n_e/n_{e,ss}$, and the normalized moles of salt removed from the separator's pores, $n_s/n_{s,ss}$, *vs.* non-dimensional time t/τ_{RC}, where the subscript ss refers to the value at the steady state. The results show that EDL charging and the electrode pore desalination are over 90% complete by about $2\tau_{RC}$. However, at this time the separator pore desalination is only about 50% complete. After about $2\tau_{RC}$, $n_s/n_{s,ss}$ slowly increases and $n_e/n_{e,ss}$ slowly decreases as salt ions are transported from the separator layer into the electrodes' pore bulk by molecular diffusion.

A key insight gained from our model predictions is that the liquid in electrodes' pores (the feed of a FTE CD cell) is desalinated at the cell's RC charging time, while the liquid in the separator (the feed of a FB CD cell) is desalinated at times significantly longer than the RC time. This is consistent with the experimental results of several other studies on FB CD systems. For example, Bouhadana *et al.* observed that upon application of a step potential to their FB CD system with a 5500 ppm NaCl feed, electrical current reached steady state (and so the cell charged) roughly 2 orders of magnitude faster than the conductivity of the feed pumped continuously through a 1 mm thick separator.[2] Bouhadana *et al.* further note that Farmer *et al.* reported similar observations of feed desalination in a FB CD system requiring significantly longer times than cell charging.[2,5] A second insight gained from our model is that salt ions initially in the separator serve to increase the salt concentration in the charged electrodes' pores, as diffusion drives salt from the separator into ion depleted electrode pores. Minimization of the separator thickness in the electric field direction can reduce this effect, and thus increase the concentration reductions achievable per charge. Such minimization is realistic in FTE designs, as the separator is not also used as the primary flow channel. From such model predictions, we conclude that FTE type architectures pose an important opportunity for CD systems to significantly reduce desalination times and increase the achievable concentration reductions of the feed stream per charge.

Experimental methods

To verify our model predictions and demonstrate the performance benefits achievable with FTE architecture, we built and characterized a prototype FTE CD cell which contained a pair of hierarchical carbon aerogel monoliths (HCAMs) as electrodes.

Electrode preparation and characterization

Our electrodes were prepared as described in detail by Baumann *et al.*, and so we will only summarize the preparation details here.[17] The aerogels were fabricated through the sol–gel polymerization of resorcinol with formaldehyde using acetic acid as a catalyst. The use of an acetic acid catalyst enabled the formation of an interconnected micron-scale pore network.[17] The nanoscale porosity was then etched into the walls of the micron-scale pore network by thermal activation in CO_2 at 950 °C. In this study, we used aerogels thermally activated for approximately 2 h. We

chose the 2 h activation time as this process resulted in a material with higher volumetric capacitance (compared to the material subjected to higher activation times). Volumetric capacitance is a key parameter in predicting desalination performance (eqn (1) and (2) use volumetric capacitance as a parameter). The HCAM material also exhibited a high porosity of about 75% as measured with saturated/dry weight measurements. We cut the material into 2 × 2 × 0.1 cm blocks which weighed 130 mg each (bulk density of 0.33 g cm^{-3}).

We characterized the pore structure of the HCAM material using mercury intrusion porosimetry (Porous Materials Inc., Ithaca, NY) (Fig. 3). The HCAM electrode exhibits a strongly bimodal pore size distribution with 70% of the pore volume attributed to pores with diameters between about 0.7 and 2 μm and 98% of the measured surface area associated with sub-10 nm pores. As total pore volume is dominated by micron-scale pores, HCAM substrates allow the liquid to flow directly through their bulk at low applied pressures. Also, the sub-10 nm pores enable a high specific capacitance (approximately 100 F g^{-1} (ref. 18)). Previous CD systems utilizing FTEs have employed electrodes of unconsolidated charcoal particle beds[10] or activated carbon paper with a strongly polydisperse macropore distribution (*e.g.*, spanning 200 to 500 nm).[15] HCAMs are, by comparison, a much more attractive choice for FTE CD electrodes, due to their monolithic structure, micron-scale pore network, and high demonstrated capacitance. Further, carbon aerogel-based electrodes have been shown to be robust to repeated charge–discharge cycling.[5,7] Note that the specific surface area measured here (see Fig. 3) reaches only about 500 m^2 g^{-1}, and this is likely because our measurement technique is limited to pores larger than about 4 nm. For example, Baumann *et al.* demonstrated approximately 1500 m^2 g^{-1} for identically fabricated HCAMs using alternate measurements of N_2 adsorption.[17]

FTE CD cell fabrication

We fabricated a FTE CD cell using two HCAM electrode blocks with macroscopic dimensions of 2 × 2 × 0.1 cm (see Fig. 4). We used a 25 μm thick, porous polypropylene separator material

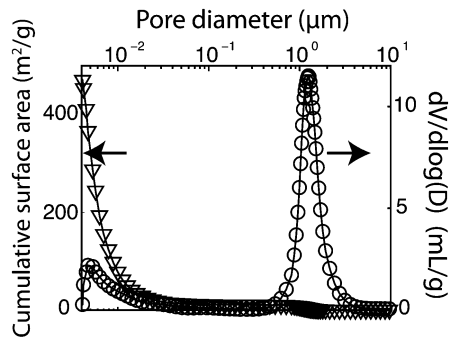

Fig. 3 Results of mercury intrusion porosimetry measurements on our HCAM material showing the cumulative surface area (left ordinance, triangles) and logarithmic volume distribution function (right ordinance, circles) *vs.* pore diameter. Pores with a diameter of approximately 1 μm contribute about 70% of the measured electrode pore volume, while the nano-scale pores provide 98% of the surface area. The unique pore structure of HCAMs enables simultaneous low hydraulic resistance and high specific capacitance.

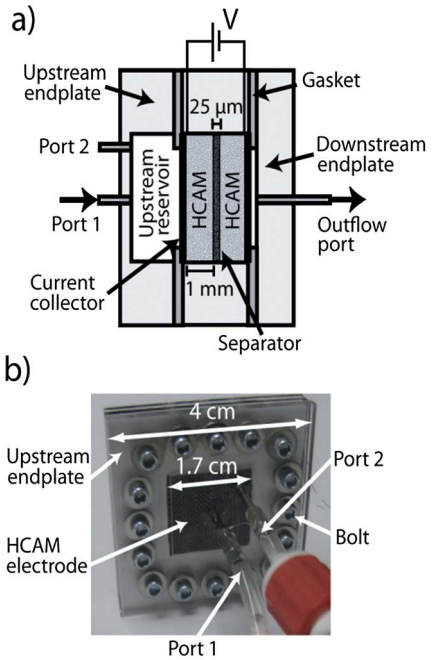

Fig. 4 (a) Schematic of the FTE CD cell used in this work and (b) image of the cell used (upstream side). The cell consisted of two 1 mm thick HCAM electrodes and a 25 μm thick porous dielectric separator. The electrode and separator assembly was epoxied into an acrylic holder, and sandwiched between upstream and downstream acrylic endplates. Teflon gaskets served to seal between acrylic components, and to hold the titanium mesh current collectors to the aerogel surface. Primary liquid flow and electric field directions were parallel and along the thin (~2 mm) dimension of the electrode and separator assembly.

(Celgard 3501, Charlotte, NC), which we inserted between the aerogels. Both the applied electric field and flow were along the smallest electrode and separator dimensions. The separator thickness was about 1% of the total electrodes-and-separator assembly, and this minimized the adverse effects of separator thickness on desalination performance (see Theory section). The electrodes and separator were sandwiched together while we epoxied this assembly into a 4 × 4 cm acrylic housing. The epoxy sealed or "potted" the assembly to the inner surfaces of the 2 × 2 cm window laser cut into the housing (Universal Laser Systems, Scottsdale, AZ), which forced pumped liquid to flow through the electrode and separator assembly. This assembly was then sandwiched between the 4 × 4 cm upstream and downstream acrylic endplates. Compressible Teflon gaskets were inserted between the assembly and the endplates, and the gaskets were laser cut to create 1.7 × 1.7 cm openings into the upstream and downstream electrode faces. We estimate the gasket thickness to be ~0.3 mm after compression of housing endplates to seal the cell. We milled the upstream endplate to accommodate a 2 × 2 × 0.2 cm reservoir space and two 1/16 inch outer diameter stainless steel tubes (Scanivalve, Liberty Lake, WA). One tube ("port 1") was used to insert the solution of interest into the upstream reservoir and/or cell assembly. The second tube ("port 2") served as an exhaust when replacing the fluid in the upstream reservoir. The downstream endplate was milled to accommodate another tubulation ("outflow port"), but had no reservoir milled into it, and so the downstream reservoir space was essentially defined by

the thickness of the compressed gasket. 2 × 2 cm titanium mesh pieces (Alfa Aesar, Ward Hill, MA) served as current collectors, and were inserted between the aerogels and Teflon gaskets. A platinum wire served to connect the titanium mesh to an external power supply (Keithley, Cleveland, OH). The entire assembly was sealed by compression using twelve 2-56 0.5 inch stainless steel bolts (Fig. 4b).

Experimental procedure

To investigate the performance of our FTE CD cell, we performed stopped flow experiments, where the charging and flow stages are sequential rather than simultaneous. The experiments proceeded as follows: we stored the cell overnight in deionized water, and then brought the cell to equilibrium prior to running experiments by flowing through it a sodium chloride solution (Harvard Apparatus syringe pump, Holliston, MA) at 0.5 mL min^{-1} for 1 h followed by three charge–discharge cycles lasting about 6 min each. The sodium chloride solution we used had concentrations of either 50, 100 or 250 mM, matching the concentration to be used in the subsequent experiment. After the repeated charge–discharge of the cell, we again pumped salt solution through the cell for 30 min. At this point, we began the experiments. First, we pumped air at 0.5 mL min^{-1} through port 1 with port 2 closed in order to empty the upstream reservoir of the sodium chloride solution. The air pump (an air-filled syringe and the syringe pump) was deactivated as soon as the reservoir was empty, to prevent drying out of the pore space. Emptying the upstream reservoir served to minimize the salt ions present outside the electrode assembly, which could potentially diffuse into the desalted electrode pores during the charging step. We then applied a step voltage across the cell, with magnitudes varying from 0.75 to 1.5 V, using a Keithley 2400 sourcemeter (Keithley, Cleveland, OH). Current response upon application of the step potential was measured at a frequency of about 1 Hz using the Keithley sourcemeter.

After charging, we extracted the desalted solution from within the electrode assembly. We performed this by pumping new (undesalted) sodium chloride solution through the cell, which displaced the desalted solution in the electrodes' pores and forced the desalted solution to exit the cell through the outlet port. To accomplish this, we first opened port 2 to exhaust the air present in the upstream reservoir while pumping new salt solution through port 1. Then, we closed port 2 and pumped new salt solution through port 1 at 0.5 mL min^{-1}, pressurizing the upstream reservoir and forcing the desalted solution out of the electrodes' pores and through the outflow port. The desalted stream exiting the cell flowed through the roughly 1 cm length of the outflow port tubulation, and then through a flow-through conductivity sensor (Edaq, Denistone East, Australia) which was calibrated to a 12.88 mS KCl standard. The conductivity sensor's internal flow channel had an ~17 μL internal volume, which allowed for a well-resolved measurement of the extracted stream conductivity. Conductivity was then transformed to concentration estimates using the Onsager–Fuoss model for molar conductivity, corrected for the effects of finite ion size (Pitts' correction).[28] The applied potential was maintained during the flow stage, except for some of the experiments described in Fig. 7 where the power source was instead disconnected from the cell during the flow stage (see Results and discussion section). After the experiment was completed, the applied potential was set to 0 V. This released salt held in the electrode EDLs. Between measurements, we pumped new salt solution for 30 min through the cell at 0.5 mL min^{-1}.

During several experiments, we also placed a pressure sensor upstream of our cell, and found that a pressure of about 10 kPa was required to maintain a 0.5 mL min^{-1} flow rate. However, a large fraction of this pressure was due to the hydraulic resistance of the thin separator (which contained pores with a diameter of about 60 nm). For example, a second test cell we built, identical to the previously described cell except containing a 125 μm thick separator with 5 μm diameter pores (Millipore, Billerica, MA), required only about 4 kPa for the 0.5 mL min^{-1} flow rate. The latter cell was not used to generate the results described in the following section.

Results and discussion

We first describe measurements of concentration of the desalted stream extracted from a fully charged FTE CD cell. In Fig. 5, we show measurements for the case of an initial NaCl concentration, c_o, of 100 mM, and for applied voltages ranging from 0.75 to 1.5 V (see Appendix B in the ESI† for similar measurements for c_o = 50 and 250 mM). The time origin in this figure represents the time when charging of the HCAM electrodes was essentially completed. That is, immediately prior to t = 0, we charged the cell for a time $5\tau_{RC}$, where τ_{RC} is the characteristic resistive–capacitive charging time of the cell (we will further describe τ_{RC} using eqn (9) and the associated text). At time t = 0 s, the pump was activated and pumped 100 mM salt solution through the cell assembly at 0.5 mL min^{-1}. Also at this time, the downstream conductivity sensor contained 100 mM salt solution. The flow induced by the pump then displaced the desalted water held in the electrodes' pores, forcing it through the downstream conductivity sensor. Fig. 5 shows measurements of concentration in this downstream sensor (see

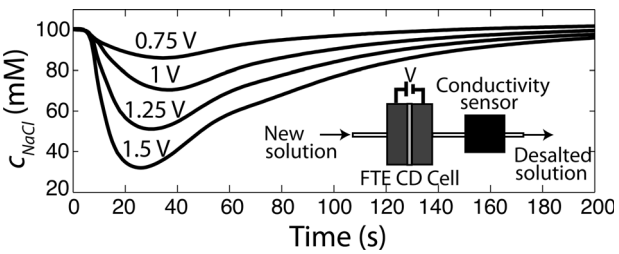

Fig. 5 Concentration of the salt solution extracted from the fully charged cell for applied voltages of 0.75 to 1.5 V, and an initial (precharge) concentration of 100 mM NaCl. The inset schematic illustrates the extraction process and shows the downstream placement of the conductivity sensor. At t = 0 s, cell charging was complete and the pump was activated, driving new 100 mM solution into the cell. The concentration then dropped as desalted water was forced out of the cell and through the sensor, reaching a minimum after about 20 s of pumping. Concentration then slowly increased as the pumped new solution completely displaced the desalted solution initially in the cell. At 1.5 V, the minimum concentration was approximately 30 mM; a reduction of 70 mM from the initial concentration.

Experimental procedure section for how we obtained concentration from conductivity measurements). In Fig. 5, we observe a fairly rapid drop in concentration soon after $t = 0$ s as desalted solution from the cell replaced the 100 mM solution initially in the conductivity sensor. For example, in the 1.5 V case, the concentration dropped from 100 to 40 mM within about 10 s. Concentrations then reached a minimum, and rose again to 100 mM after an order of 100 s readjustment time. This readjustment occurred as the desalted solution in the cell approached complete displacement by the new 100 mM solution. Note the expected decrease in minimum measured concentration, c_{min}, with increasing voltage. At 1.5 V, c_{min} was about 30 mM, yielding a concentration reduction, $\Delta c = c_o - c_{min}$, of about 70 mM for a single charge.

The observed slow readjustment is consistent with strong dispersion of the interface between the desalted solution initially in the cell and the new 100 mM solution then pumped through the cell. We extracted the desalted solution from the cell *via* miscible displacement through the porous electrode–separator assembly. Miscible displacement in porous media is often characterized by a disperse interface between initial and replacing liquids, and mixing can be due to mechanical dispersion (mixing due to flow through an interconnected, random pore structure).[29] Minimizing this dispersion is desirable for efficient operation of FTE CD cells, especially for stopped flow operation. Thus, our results highlight that future work on FTE CD systems should attempt to minimize dispersion through further optimizations of flow and system geometric parameters.

We also performed experiments similar to those of Fig. 5, but for initial salinities, c_o, of 50 and 250 mM. In Fig. 6, we show measured concentration reduction, Δc, *vs.* applied potential for various c_o. The data shows several trends. Firstly, at the higher c_o values of 100 mM and 250 mM, Δc scaled approximately linearly with applied voltage. However, at $c_o = 50$ mM, Δc plateaued at potentials above 1 V, as it approached the maximum achievable value of 50 mM. This indicates that at $c_o = 50$ mM and above 1 V we removed nearly all salt from the feed solution in the cell. Second, we observed that Δc increased by a factor of approximately 7 when we doubled voltage from 0.75 to 1.5 V for c_o values of 100 and 250 mM. We attribute this strong dependence of Δc with applied voltage to a combination of the following effects: the increased equilibrium potential across the pore EDLs which enables additional charge storage; the measured increase of electrode charge efficiency with potential between 0.75 and 1.25 V (see Appendix B in the ESI†); and the measured increase of cell capacitance with increasing potential (see Appendix B).

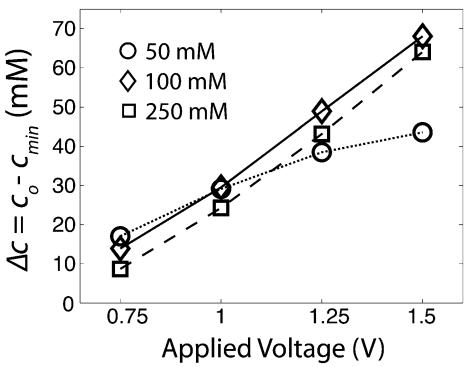

Fig. 6 Measured concentration reduction, Δc, *vs.* applied voltage for initial NaCl concentrations, c_o, of 50, 100 and 250 mM. At the higher c_o of 100 mM (diamonds, solid line) and 250 mM (squares, dashed line), Δc scaled approximately linearly with the potential, and Δc increased by a factor of approximately 7 for a 2× increase in voltage. For a c_o of 50 mM (circles, dotted line), Δc instead plateaued at high potentials as it approached its maximum achievable value of 50 mM.

We further characterized our FTE CD cell by calculating its RC time constant at the twelve experimental conditions of Fig. 6 ($c_o = 50$, 100, 250 mM, and $V = 0.75$, 1, 1.25, 1.5 V). Eqn (4) provides an estimate for the RC time constant using the geometric dimensions of the electrodes and separator, and the porosity and tortuosity of the electrodes and separator (which were assumed equal). However, a more accurate calculation of our cell's RC time constant can be made with an *in situ* measurement of the series resistance, R_s (resistance of the separator and any contact resistances), and a measurement of the cell's capacitance, C_{cell}. The measurement of R_s can be obtained by dividing the applied voltage, V, by current measured upon application of the step potential, i_o, as initially, the entire applied potential is dropped across R_s (see Fig. 2b).[30] Thus, our cell's RC time constant, τ_{RC}, can be calculated with the following equation:

$$\tau_{RC} = \left(\frac{2l_e T_e}{\psi_e A \sigma_o} + \frac{V}{i_o}\right) C_{cell}. \quad (9)$$

Here A is the electrode cross-sectional area, ψ_e, is the porosity of the electrodes, and T_e represents the tortuosity of the electrodes. C_{cell} was obtained from measurements of our cell's current response (see Appendix B in the ESI†). C_{cell} increased with both the applied potential and the sodium chloride concentration, with a minimum of 4.8 F at 0.75 V, 50 mM and a maximum of 8.4 F at 1.5 V, 250 mM NaCl. A cell capacitance of 8.4 F corresponds to a specific capacitance of a single HCAM electrode of nearly 130 F g^{-1} or 40 F cm^{-3}. Note that for equally sized electrodes, the gravimetric capacitance of a single electrode is estimated as four times the gravimetric capacitance of the cell.[31] We calculated T_e from measurements of the pressure required to flow through our electrodes (see Appendix B in the ESI† for calculations) and obtain $T_e = 3.6$. This is consistent with reports of the tortuosity of porous carbon structures (including aerogels and activated carbons) which have typical values of 3 to 4.[32,33] The τ_{RC} of our cell increased with increasing voltage and decreasing initial NaCl concentration, and varied from 81.6 s at 0.75 V and 250 mM to 350.1 s at 1.5 V and 50 mM.

In the inset of Fig. 7 we plotted measurements of charge stored in the EDL, q, *vs.* charging time, t, for the twelve experimental conditions used in Fig. 6 (thin black lines and associated markers, see legend). q was obtained by applying a step potential to the cell at $t = 0$, and integrating the measured current *vs.* time data. Before integration, a leakage current, defined as the current at $5\tau_{RC}$ (here current decreased by about 1% per minute), was subtracted from the current signal. Leakage current increased with voltage and ionic strength from about 300 μA at 0.75 V and 50 mM to over 4 mA at 1.5 V and 250 mM, and was less than 1% of initial current, i_o, for all experimental conditions. All q *vs.* t curves exhibited an initial rapid increase, and then plateaued past

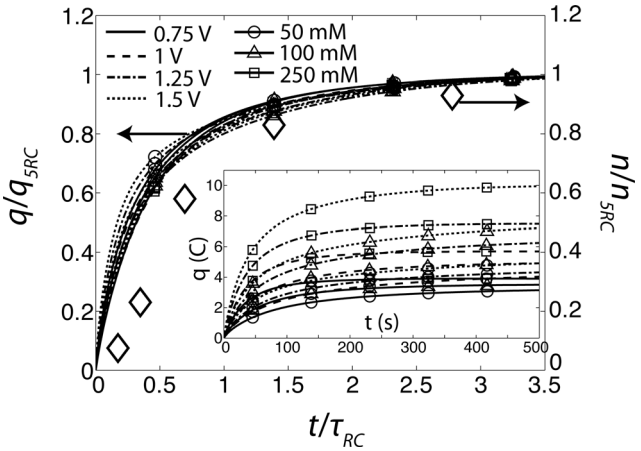

Fig. 7 Non-dimensional charge stored at electrode EDLs, q/q_{5RC} (left ordinate), and non-dimensional moles of salt removed from the cell, n/n_{5RC} (right ordinate) *vs.* scaled time, t/τ_{RC}. q/q_{5RC} data are plotted for applied voltages from 0.75 to 1.5 V with initial salinities of 50 to 250 mM NaCl (thin, marked black lines, see legend). We also plot n/n_{5RC} for an initial salinity of 100 mM and 1 V applied voltage (diamonds). The inset plot shows the dimensional charge stored, q, *vs.* time. Scaling time with τ_{RC} resulted in a collapse of all q/q_{5RC} curves, and EDL charging was in all cases about 90% complete by $2\tau_{RC}$. n/n_{5RC} shows roughly the same trend as observed for q/q_{5RC} curves. The latter two results indicate that both cell charging and electrode pore desalination occurred at an RC timescale, as predicted by our model (see Theory section).

a time of the order 100 s as EDL charging approached completion. One key conclusion from our model results was that both EDL charging and electrode pore desalination occur at RC timescales (see Theory section). Based on this insight, in the main axis of Fig. 7, we plotted normalized charge *vs.* time non-dimensionalized by τ_{RC} (thin black lines as per legend), with τ_{RC} determined for each experimental condition using eqn (9). Charge stored values were normalized by that stored at $t = 5\tau_{RC}$, q_{5RC}. This scaling approximately collapsed all of the q *vs.* t curves. Further, for all conditions, q/q_{5RC} was about 0.90 by $2\tau_{RC}$. This result demonstrates that the EDL charging process of our cell is well described by the cell's RC time constant.

In the main plot of Fig. 7 we further show measurements of non-dimensional moles of salt removed from the liquid in the cell, n/n_{5RC}, *vs.* t/τ_{RC} for the case of $c_o = 100$ mM and 1 V applied potential (diamonds). We obtained the latter experimental data by charging the cell to prescribed times (equivalent to about 0.2, 0.35, 0.7, 1.4, 2.75, and $5\tau_{RC}$), and then extracting the desalted solution from the cell using the miscible displacement technique described previously (see Fig. 5), with the power supply disconnected from the cell during extraction. We then calculated n by integrating the concentration *vs.* time curves measured by the downstream conductivity sensor, and multiplying this by the constant flow rate used during extraction (here 0.5 mL min^{-1}). We observed that the n/n_{5RC} data are similar to the q/q_{5RC} curves, as n/n_{5RC} rose quickly between about $t = 0$ to τ_{RC}, and then levelled off past about τ_{RC}. These observations confirm that the RC timescale also well describes desalination of the feed solution in our FTE CD cell, as predicted by our model. These desalination dynamics are in stark contrast to measurements reported by studies on FB CD systems, where desalination required over an order of magnitude longer time than cell charging.[2] Thus, these results further highlight the potential for FTE CD to provide for significantly faster desalination than typical FB CD cells.

We note that at times less than τ_{RC}, EDL charging progressed to a greater degree than desalination. For example, at $t = 0.35\tau_{RC}$, q/q_{5RC} is about 0.6, while n/n_{5RC} is about 0.25. A disparity in the progression of stored electric charge *vs.* measurable amounts of desalting is characteristic of the transient charging of a Gouy–Chapman EDL,[6] demonstrating that future works should use more realistic EDL structure models to capture exact FTE CD cell performance.

In Table 1, we compare our prototype FTE cell to several recently developed FB systems.[2,7,34] These systems employed electrodes of mesoporous carbon,[34] activated carbon cloth,[2] or traditional carbon aerogel,[7] and the electrode mass used, m_e, is given in Table 1. Relative to these systems, our device exhibits 4 to 10 times higher mean sorption rate, r, defined as the average rate of salt removed during the desalination stage normalized by the weight of the electrodes.[7] Xu *et al.* report the mean sorption rate for various feed salinities and flow rates, with a maximum reported rate of about 0.1 mg TDS per g carbon per min.[7] We estimated r for the systems of Bouhadana *et al.* and Tsouris *et al.* from their measurements of the amount of salt removed from the feed, electrode mass, and the times required for desalination.[2,34] We estimate $r \sim 0.1$ mg NaCl per g carbon per min from Fig. 5 of Bouhadana *et al.*,[2] and $r \sim 0.25$ mg TDS per g carbon per min from Fig. 6b and Table 1 of Tsouris *et al.*[34] For our system, we calculated r by normalizing n_{5RC} by the weight of both electrodes and $5\tau_{RC}$, as salt uptake was essentially complete by $5\tau_{RC}$ (Fig. 7). The maximum mean sorption rate that we obtained was 0.96 mg NaCl per g aerogel per min at 1.25 V and 250 mM NaCl. We note that our cell can likely achieve higher mean sorption rates by charging for shorter times, such as 2 or $3\tau_{RC}$, as little additional salt is retained in the EDLs past about $2\tau_{RC}$. At 1.25 V and 250 mM, our cell removed 7.5 mg NaCl per g aerogel, roughly equivalent to the sorption achieved with previous FB CD systems using carbon aerogel electrodes.[7] The maximum sorption exhibited by our cell occurred at 1.5 V and 100 mM, and was 10.2 mg NaCl per g aerogel. Other electrode materials, such as mesoporous carbons, have achieved higher sorption, but lack the micron-scale pore network needed for efficient flow-through.[34] Also, as shown in Table 1, the separator-to-electrode thickness ratio, $l_s/2l_e$, is typically about unity for FB systems, but is 0.01 for our FTE system. FB systems require the separator to act as a flow channel, leading to large thickness ratios. In our FTE architecture, we no longer require the separator to be a primary flow channel, allowing us to minimize the separator thickness to reduce the cell volume and ionic resistance.

We note that our cell was operated at potentials up to 1.5 V, while systems shown in Table 1 were operated from 1.1 to 1.3 V. Previous studies have noted that feed conductivity reductions worsen for potentials above about 1.2–1.3 V.[34] In contrast, we observed a monotonic increase in Δc up to our highest applied potential of 1.5 V (Fig. 5). This indicates that our HCAM electrodes were more effective in avoiding performance degradation due to electrochemical reactions, such as the hydrogen and oxygen evolution reactions. We hope to explore the nature and rate of these electrochemical reactions, and the stability of our HCAM electrodes at high potentials in a future work.

Table 1 Comparison of system characteristics and performance between the FTE CD system presented here and several recently developed FB CD systems.[2,7,34] Our system demonstrated a 4 to 10 times higher mean sorption rate, r, and utilized a separator-to-electrode thickness ratio, $l_s/2l_e$, two orders of magnitude smaller than that of the FB CD systems

	m_e [g]	$l_s/2l_e$ (l_e [mm])	Feed	V [V]	r [mg TDS per g carbon per min]
Xu *et al.* (2008)	650	1.4 (0.81)	5000 ppm NaCl	1.3	0.1
Bouhadana *et al.* (2010)	14	1.5 (0.5)	5500 ppm NaCl	1.1	0.1
Tsouris *et al.* (2011)	9.6	[a]	5000 ppm Instant ocean	1.2	0.25
Current work	0.26	0.01 (1)	250 mM NaCl	1.25	0.96

[a] l_e not reported, $l_s = 6$ mm.

Conclusions

Using macroscopic porous electrode theory coupled with the transient charging of a Helmholtz EDL, we demonstrated that desalination of the feed of a FB CD cell can require much longer times than cell charging and desalination of electrode pores. We designed, built, and tested a novel FTE CD cell where the feed volume is instead within the electrode pores. This cell leverages newly developed hierarchical carbon aerogel monoliths as an electrode material. These electrodes are well suited for FTE applications as they combine the inherent benefits of a monolithic aerogel material with a pore structure that enables both low fluidic resistance and high specific capacitance. Our experiments validated the timescale trends predicted by our model by demonstrating that desalination in FTE architecture occurs at the cell charging (RC) timescale. We also demonstrated a feed concentration reduction of up to 70 mM NaCl and a mean sorption rate 4 to 10 times higher than that typically achieved with FB CD systems.

Acknowledgements

This work was supported by the National Science Foundation under grant no. 0967600 and State of California's Proposition 50 funds administered by the Department of Water Resources. Any opinions, findings, and conclusions or recommendations expressed in this material are those of the authors and do not necessarily reflect the views of the National Science Foundation. MES would like to thank the Lawrence Scholar program and a postgraduate scholarship from the Natural Sciences and Engineering Research Council (NSERC) of Canada. Work at LLNL was performed under the auspices of the US DOE by LLNL under Contract DE-AC52-07NA27344.

Notes and references

1 M. A. Shannon, P. W. Bohn, M. Elimelech, J. G. Georgiadis, B. J. Marinas and A. M. Mayes, *Nature*, 2008, **452**, 301–310.
2 Y. Bouhadana, E. Avraham, A. Soffer and D. Aurbach, *AIChE J.*, 2010, **56**, 779–789.
3 Y. Oren, *Desalination*, 2008, **228**, 10–29.
4 M. A. Anderson, A. L. Cudero and J. Palma, *Electrochim. Acta*, 2010, **55**, 3845–3856.
5 J. C. Farmer, D. V. Fix, G. V. Mack, R. W. Pekala and J. F. Poco, *J. Electrochem. Soc.*, 1996, **143**, 159–169.
6 P. M. Biesheuvel and M. Z. Bazant, *Phys. Rev. E: Stat., Nonlinear, Soft Matter Phys.*, 2010, **81**, 031502.
7 P. Xu, J. E. Drewes, D. Heil and G. Wang, *Water Res.*, 2008, **42**, 2605–2617.
8 S. Porada, L. Weinstein, R. Dash, B. van der Wal, M. Bryjak, Y. Gogotsi and P. M. Biesheuvel, *ACS Appl. Mater. Interfaces*, 2012, **4**, 1194–1199.
9 D. Brogioli, R. Zhao and P. M. Biesheuvel, *Energy Environ. Sci.*, 2011, **4**, 772–777.
10 A. M. Johnson, A. W. Venolia, J. Newman, R. G. Wilbourne, C. M. Wong, W. S. Gilliam, S. Johnson and R. H. Horowitz, *The Office of Saline Water Research and Development*, Progress Report No. 516, US Dept. of the Interior, Publication 200 056, 1970.
11 A. M. Johnson and J. Newman, *J. Electrochem. Soc.*, 1971, **118**, 510–517.
12 E. Avraham, Y. Bouhadana, A. Soffer and D. Aurbach, *J. Electrochem. Soc.*, 2009, **156**, P95–P99.
13 E. Avraham, M. Noked, Y. Bouhadana, A. Soffer and D. Aurbach, *J. Electrochem. Soc.*, 2009, **156**, P157–P162.
14 E. Avraham, M. Noked, Y. Bouhadana, A. Soffer and D. Aurbach, *Electrochim. Acta*, 2010, **56**, 441–447.
15 I. Cohen, E. Avraham, M. Noked, A. Soffer and D. Aurbach, *J. Phys. Chem. C*, 2011, **115**, 19856–19863.
16 T. Humplik, J. Lee, S. C. O'Hern, B. A. Fellman, M. A. Baig, S. F. Hassan, M. A. Atieh, F. Rahman, T. Laoui, R. Karnik and E. N. Wang, *Nanotechnology*, 2011, **22**, 292001–292019.
17 T. F. Baumann, M. A. Worsley, T. Y. J. Han and J. H. Satcher, *J. Non-Cryst. Solids*, 2008, **354**, 3513–3515.
18 J. Biener, M. Stadermann, M. Suss, M. A. Worsley, M. M. Biener, K. A. Rose and T. F. Baumann, *Energy Environ. Sci.*, 2011, **4**, 656–667.
19 R. T. Mayes, C. Tsouris, J. O. Kiggans Jr, S. M. Mahurin, D. W. DePaoli and S. Dai, *J. Mater. Chem.*, 2010, **20**, 8674–8678.
20 J. Newman and K. E. Thomas-Alyea, *Electrochemical Systems*, John WIley & Sons, Inc., Hoboken, NJ, 2004.
21 R. J. Hunter, *Zeta Potential in Colloidal Science, Principles and Applications*, Academic Press, New York, 1981.
22 R. Zhao, P. M. Biesheuvel, H. Miedema, H. Bruning and A. van der Wal, *J. Phys. Chem. Lett.*, 2009, **1**, 205–210.
23 M. Z. Bazant, M. S. Kilic, B. D. Storey and A. Ajdari, *Adv. Colloid Interface Sci.*, 2009, **152**, 48–88.
24 P. M. Biesheuvel, Y. Fu and M. Z. Bazant, *Phys. Rev. E: Stat., Nonlinear, Soft Matter Phys.*, 2011, **83**, 061507.
25 M. S. Kilic, M. Z. Bazant and A. Ajdari, *Phys. Rev. E: Stat., Nonlinear, Soft Matter Phys.*, 2007, **75**, 021502.
26 M. S. Kilic, M. Z. Bazant and A. Ajdari, *Phys. Rev. E: Stat., Nonlinear, Soft Matter Phys.*, 2007, **75**, 021503.
27 R. de Levie, *Electrochim. Acta*, 1963, **8**, 751–780.
28 S. S. Bahga, M. Bercovici and J. G. Santiago, *Electrophoresis*, 2010, **31**, 910–919.
29 F. A. L. Dullien, *Porous Media: Fluid Transport and Pore Structure*, Academic Press, San Diego, 1992.
30 B. E. Conway, *Electrochemical Supercapacitors*, Kluwer Academic/Plenum Publishers, New York, 1999.
31 M. D. Stoller and R. S. Ruoff, *Energy Environ. Sci.*, 2010, **3**, 1294–1301.
32 D. Jayne, Y. Zhang, S. Haji and C. Erkey, *Int. J. Hydrogen Energy*, 2005, **30**, 1287–1293.
33 R. Leyva-Ramos and C. J. Geankoplis, *Can. J. Chem. Eng.*, 1994, **72**, 262–271.
34 C. Tsouris, R. Mayes, J. Kiggans, K. Sharma, S. Yiacoumi, D. DePaoli and S. Dai, *Environ. Sci. Technol.*, 2011, **45**, 10243–10249.
35 O. Heaviside, *Electromagnetic Theory*, Chelsea Pub. Co., New York, 1971.
36 R. Zhao, P. M. Biesheuvel and A. van der Wal, *Energy Environ. Sci.*, 2012, DOI: 10.1039/c2ee21737f.